Construction and Calibration of Optically Efficient LCD-based Multi-Layer Light Field Displays

Matthew Hirsch, Douglas Lanman,
Gordon Wetzstein, Ramesh Raskar

MIT Media Lab, Building E14, 75 Amherst St. Cambridge, MA, 02139, USA

E-mail: mhirsch@media.mit.edu

Abstract. Near-term commercial multi-view displays currently employ ray-based 3D or 4D light field techniques. Conventional approaches to ray-based display typically include lens arrays or heuristic barrier patterns combined with integral interlaced views on a display screen such as an LCD panel. Recent work has placed an emphasis on the co-design of optics and image formation algorithms to achieve increased frame rates, brighter images, and wider fields-of-view using optimization-in-the-loop and novel arrangements of commodity LCD panels. In this paper we examine the construction and calibration methods of computational, multi-layer LCD light field displays. We present several experimental configurations that are simple to build and can be tuned to sufficient precision to achieve a research quality light field display. We also present an analysis of moiré interference in these displays, and guidelines for diffuser placement and display alignment to reduce the effects of moiré. We describe a technique using the moiré magnifier to fine-tune the alignment of the LCD layers.

1. Introduction

Though holography may one day produce life-like 3D video displays, current state-of-the-art holographic displays face difficult trade-offs between spatial resolution, refresh rate, field-of-view, and cost. These shortcomings in the capabilities of holographic video technology, however temporary, have allowed a wide variety of ray-based 3D and 4D light field displays to find academic and limited commercial success. Conventional approaches to ray-based display typically include lens arrays [1] or heuristic barrier patterns [2] combined with integral interlaced views on a display screen such as an LCD panel.

Recent work [3] has placed an emphasis on the co-design of optics and image formation algorithms to achieve increased frame rates, brighter images, and wider fields of view using optimization-in-the-loop and novel arrangements of commodity LCD panels. We have dubbed this emerging field computational display, as it has, in part, grown out of the computational camera community. We have previously demonstrated computational displays that are compressive in nature, in that fewer parameters are configured on the display hardware than unique rays generated.

In this paper we examine the construction and calibration methods of computational, multi-layer LCD-based light field displays. We present several experimental configurations that are simple to build and can be tuned to sufficient precision to achieve a research quality light field display. The optical configurations were employed in our *Polarization Fields* [4] and *Tensor Display* [3] papers. Here we focus on their construction and calibration. We present an analysis

of moiré – spatial frequency aliasing caused by the interference of pixel grids at different distances – and an analysis of diffuser placement and display alignment to reduce the effects of moiré. Finally, we describe a technique using the moiré magnifier [5] to fine-tune the alignment of the LCD layers.

2. Related Work

Conventional light field display has its roots in integral imaging [1] and parallax barriers [2], developed over a century ago. Since that time, commercial products such as the Nintendo 3DS[1] or Alioscopy glasses-free television[2] have continued to use barriers and cylindrical lens sheets, respectively, to produce stereo pairs for glasses-free viewing. These decisions are motivated by cost and the unavoidable spatial resolution loss imposed by these simple techniques.

Though switchable liquid crystal lenses[6] have begun to achieve commercial success in combining high resolution 2D display and lower resolution 3D display in a single unit, they do not address the resolution loss in integral imaging systems. Viewer-adaptive barrier patterns [7], and time sequential barrier patterns [8] can increase resolution or field-of-view for general light field display, and simple formulations for stacked LCD panels can represent limited depth at full resolution [9], but it is only recently that fast switching LCD panels and high performance graphics hardware has made it possible to address general purpose, content adaptive barrier patterns [10]. Generalizing the problem of light field display has proven a productive research direction, with recent work demonstrating both light-efficient, multi-layer designs [4, 11, 12], and formulations that incorporate multi-layer panels, directional backlighting, and temporal multiplexing [3].

3. Display Architectures

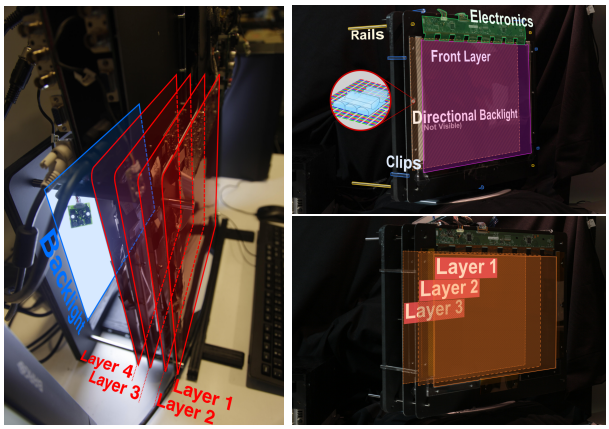

Figure 1. (Left) Polarization Field prototype. This display is composed of four linear polarization state rotators, surrounded by a pair of crossed linear polarizers. (Right) Tensor Displays. (Top) Two-layer directional backlight Tensor Display, an optically efficient design. (Bottom) Three-layer Tensor Display, composed of three high-speed attenuation-mode LCD panels.

In this section, we describe the construction of two optically efficient light field display prototypes. Both of the presented prototypes use optically efficient designs made possible by our computational image formation models, presented in our Polarization Fields [4] and Tensor Displays [3] works.

3.1. Polarization Fields

The light-efficient optical configuration of the Polarization Fields display is allowed only by the reformulation of the light field synthesis equation (Equation 2) in terms of a stack of linear

[1] http://www.nintendo.com/3ds
[2] http://www.alioscopy.com

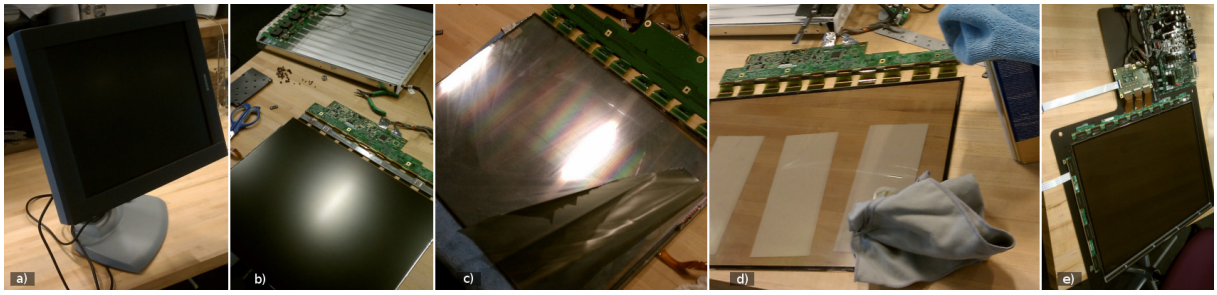

Figure 2. We disassemble a Barco E-2320 PA panel to convert it from an attenuation based display to a linear polarization state rotating element. a) Assembled. b) Panel removed from case. c) Removing the diffusing, linear polarizing films. d) Cleaning adhesive residue with acetone and microfiber cloth. d) Stripped and cleaned panel mounted to CNC cut aluminum frame.

polarization state rotators. In turn, a stack of bare, liquid crystal panels could be constructed and modeled in many ways, but using our simplified linear polarization state rotator model, solving the image synthesis problem for this stack is amenable to fast linear methods that run in real time on modern GPUs [13].

3.1.1. Synthesis In our Layered 3D paper [14], we introduced a light field image formation model for devices composed of attenuating layers. We cast the problem of light field display from a device composed of attenuating layers as an iterative back projection problem, in which the views of the desired light field are modeled as projections through the volume of layers. In order to linearize the problem, we solve for the light field in log space, as

$$\arg\min_{\alpha} \|\bar{\mathbf{l}} + \mathbf{P}\alpha\|^2, \text{ for } \alpha \geq 0, \tag{1}$$

where $\bar{\mathbf{l}}$ denotes the log light field, $\mathbf{P}$ the projection matrix through the display stack, and α a vector of mask values. However, it is impractical to apply these methods to LCDs directly, as LCD transmissivity is low when polarizing sheets surround the LC panel.

In Polarization Fields, we reformulate our image formation model to function in polarization rotation space, modeling a bare LC panel as a linear polarization state rotator [15]. This allows us to construct a stack of optically efficient liquid crystal layers (Figure 1, (Left)). The entire stack is surrounded by one pair of crossed linear polarizers, and illuminated by a uniform backlight. As before, our formulation is posed as an iterative backprojection problem,

$$\arg\min_{\phi} \|\theta - \mathbf{P}\phi\|^2, \text{ for } \phi_{min} \leq \phi \leq \phi_{max}, \tag{2}$$

where θ denotes the linear polarization state rotation angles, per ray, necessary to create a desired light field after interaction with a linear polarizing analyzer, via Malus' law.

As in Equation 1, $\mathbf{P}$ denotes the projection matrix through the polarization fields display stack. ϕ is a vector of polarization rotation values, per layer.

3.1.2. Construction Our prototype was built using off-the-shelf components. We disassemble four Barco E-2320 PA LCD panels, removing the backlights and polarizing films (Figure 2). As these panels are medical grayscale panels, they contain no color filters. Color is theoretically restored to the display using a time sequential backlight.

The disassembled display panels are mounted CNC cut aluminum frames, which slide on precision steel rails. The rails are aligned inside a wooden, CNC machined frame. Final alignment is done using the technique described in Section 4.1.2. Light fields are not displayed at the full spatial resolution of the panel due to computational hardware constraints. This affords additional misalignment tolerance to the system.

3.2. Tensor Displays

In Tensor Displays, we further generalize the problem of light field display through attenuating layers to account for temporal modulation using high speed displays, as well as variation across layers. In addition, our Tensor Display formulation allows new refractive optical elements, such as a directional backlight.

3.2.1. Synthesis We refer readers to our Tensor Display paper [3] for complete documentation. Here, we outline the synthesis as it enables the construction of an optically-efficient light field display. The central observation of the framework is that the choice of an *absolute coordinate system* allows a light field displayed from a multi-layer device to be restricted to a N^{th}-order, rank-M tensor, where the order of the tensor, N, is determined by the number of layers in the multi-layer display, and the rank of the tensor, M, is determined by the number of time steps available. The layer values at each time step are then determined as the result of a Non-negative Tensor Factorization [16] (NTF). For the general case

$$\underset{\{\mathbf{F}^{(n)}\}}{\arg\min} \left\| \mathcal{L} - \mathcal{W} \circledast \tilde{\mathcal{T}} \right\|^2, \text{ for } 0 \leq \mathbf{F}^{(n)} \leq 1, \tag{3}$$

where $\tilde{\mathcal{T}} = [\![\mathbf{B}, \mathbf{F}^{(1)}, \mathbf{F}^{(2)}, \ldots, \mathbf{F}^{(N)}]\!]$. $\mathbf{B}$ is the light field emitted by the directional backlight, and $\mathbf{F}^{(N)}$ is a vector of attenuation values placed on the N^{th} layer of the display.

3.2.2. Construction The flexibility of the Tensor Display image synthesis framework allows for a variety of hardware configurations. In Figure 1 (Right), (Top) and (Bottom), our prototype is show configured in a two-layer, directional backlight mode, and a three-layer, uniform backlight mode, respectively. The Tensor Display framework does not yet handle polarization rotation, as in Polarization Fields, but allows an alternative light-efficient configuration in the form of the two-layer, directional backlight display.

Construction of the Tensor Display prototype closely follows that of the Polarization Fields prototype described in Section 3.1.2, but differs in a few key design choices. Rather than grayscale medical panels, we use high speed (120HZ) Viewsonic VX2268wm LCDs. These panels are intended for use with shutter glasses, and so have fast response times with little ghosting. Because we use these panels in attenuation mode, we place a linear polarizer at the rear of the stack, and successively crossed linear polarizers at the face of each panel.

In the light-efficient two-layer directional backlight configuration we employ a lens array to create a generic low resolution light field display for use as the directional backlight component. We implement our lens array by placing two crossed 1D lenticular sheets atop one another, such that the first sheet is rotated 90° and facing inward (Figure 1, Inset). We use a 10 lens-per-inch sheet from Microlens Technologies. The use of cheap lens sheets in this configuration is not ideal, as it results in scattering at the lens edges, creating a dark grid in the resulting images. The placement of the top lens sheet above the bottom lens sheet imposes a small astigmatism, as the top sheet is not one focal length distance from the rear LCD screen. The lenses we use are not polarization preserving, and require an additional linear polarizer between the front of the lens sheet and the rear of the top LCD screen. Each of the aforementioned issues can be resolved with more sophisticated engineering.

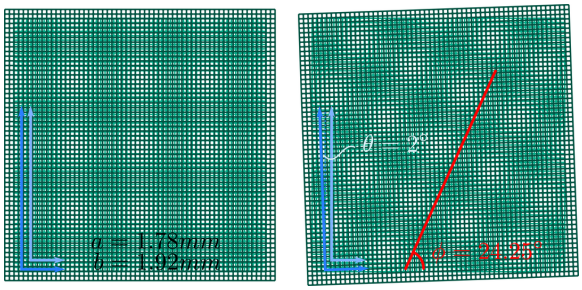

Figure 3. Moiré interference patterns caused by scaled and rotated grids. Best viewed at full resolution. The grids differ in pitch by 7%. On the right, the larger grid is rotated by $\theta = 2°$, causing an apparent rotation of the moiré fringes by $\phi = 24.25°$.

4. Considering Moiré

4.1. Calibration

Moiré fringes are observed when two patterns of different spatial frequency are multiplied. The effect is often observed in digital photography and display when patterns in a scene approach the spatial frequency of the underlying pixel grid of the image capture or display device. From a signal processing perspective, Moiré can be understood as a beat frequency between signals of similar spatial frequencies, or equivalently, spatial frequency aliasing. In this section, we demonstrate how to use moiré fringes to accurately align layered lens array and LCD systems.

4.1.1. Lenticular Alignment In many light field displays, including our two-layer Tensor Display (Section 3.2), it is necessary to align a lenticular sheet or lens array to an underlying pixel grid. Here we described a simple technique to perform rotational alignment using the moiré effect. In the case of lens sheets, this effect has been succinctly described as the *moiré magnifier* [5]. Following Hutley et. al., an expression can be obtained for the relative rotation and magnification of the image of the pixel grid of the LCD panel as viewed through the lens array. For convenience, we reproduce Hutley et. al.'s magnification, m and rotation, ϕ, here, with one minor modification: we simplify the denominator using the Pythagorean trigonometric identity.

$$m = \frac{a}{\sqrt{a^2 + b^2 - 2ab\,\cos(\theta)}} \tag{4}$$

$$\sin(\phi) = \frac{-b\,\sin(\theta)}{\sqrt{a^2 + b^2 - 2ab\,\cos(\theta)}} \tag{5}$$

As we show numerically below, for practical values of LCD and lens pitch, small rotations of the lens array will be magnified in the moiré pattern. The calibration task reduces to leveling the perceived moiré fringes by eye. If the lens pitch is nearly an integer multiple of the LCD pitch, as is the desired case, then m will be nearly infinite when $\theta = 0$. Moiré bands will not be visible under these conditions. However this calibration technique applies equally to patterns displayed on the LCD as the pixel structure of the screen itself. It is often desirable to display a pattern on the LCD to improve the contrast of the observed moiré pattern. Once the pattern has been leveled by rotating the lens sheet, the pitch of the lens sheet can be calibrated by adjusting the pitch of repeating pattern displayed on the LCD until m is infinite, or equivalently, no fringe patterns are visible. In the case of a research prototype using an imperfectly matched lens array and LCD panel, the displayed pattern may be interpolated to achieve sub-pixel alignment, with a small angular cross-talk penalty in the resulting light field display.

To determine the expected accuracy of the above method, we consider the physical values from our Tensor Display prototype. The lens pitch is $a = 2.54mm$, and LCD pixel pitch is $b = 282\mu m$. We found that the rotation of the moiré fringes could be aligned to within $\phi = 0.5°$. Substituting into Equations 5 and 4, and solving for θ and m, respectively, we get $\theta = 4°$ and $m =$ undefined. This is a result of choosing a and b as nearly integer multiples ($a/b = 9.007$), and

indicates that alignment by eye will not be very accurate. To improve accuracy, we can display a linearly interpolated pattern on the LCD with a pitch of $b = 2.1mm$. Now, for $\phi = 0.5°$, $m = 5.77$ and $\theta = 0.105°$, allowing nearly $5\times$ improvement in accuracy over alignment by eye.

4.1.2. LCD Alignment Though it is possible to use the scale of moiré fringes to perform alignment in depth, we find it is much simpler in practice to use CNC machines to cut spacer clips, which can fasten to multiple layers of optical elements and space them accurately to the tolerance of the CNC machine – $0.25mm$ or less. In this section, as in Section 4.1.1, we will concentrate primarily on rotational alignment of LCD panels, to which moiré fringes are more sensitive.

Though the analysis of Section 4.1.1 was derived from the *moiré magnifier* effect of lens arrays, we observe that Equations 4 and 5 apply equally to lens arrays and grid patterns. Oster et. al. [17] use an analysis based on indical representations of curves to derive Equations 6 and 7 in their paper for moiré fringe pitch and rotation, which match our Equations 4 and 5, save for a sign difference. We show in Figure 3 that the analysis holds for a printed grid pattern.

When aligning LCD screens spaced by a distance d_s, the difference in pixel size Δp, observed by a viewer at distance d_o is due to perspective projection. By similar triangles,

$$\Delta p = \frac{pf}{d_o} - \frac{pf}{d_o + d_s}. \tag{6}$$

where f is the focal length of the human eye, accepted to be approximately $22mm$. For the physical dimensions of our three-layer Tensor Display prototype (considering the front two layers) $p = 282\mu m$, $d_o = 1m$, $d_s = 4cm$, we calculate that $\Delta p = 0.241\mu m$. Substituting the two apparent LCD pitches into Equation 5, we find that a pattern rotation of $\phi = 0.5°$ yields a screen rotation of just $\theta = 7.5 \times 10^{-6}$ degrees, indicating that aligning the LCD layers by straightening the visible moiré fringes will achieve very accurate alignment. It is useful to note that, with such a small difference in pitch, the magnification, m, will be large, making it more difficult to achieve accurate visual rotation alignment. Thus, $\phi = 0.5°$ may be an overly generous estimate.

4.2. Mitigation

While moiré is beneficial for accurate calibration, it is an unpleasant visual nuisance when observing a light field. In order to eliminate moiré, one need only prevent the multiplication of similar spatial frequency signals. We find that there are two approaches that can mitigate moiré:

- Achieve a small magnification factor, m, such that aliased copies of the signal are small relative to image features
- Implement a spatial low-pass or notch filter to remove the offending frequencies

In the case of LCD panels, the first of the above strategies implies separating the panels by a large distance. Larger separation increases Δp from Equation 6. However, a large separation distance is not always practical, and does not apply to lenticular sheets and lens arrays.

The second approach can be achieved in two-layer and lenticular devices by placing an appropriately chosen diffuser on the rear LCD layer. An appropriate diffuser choice will impose a spatial frequency cut-off such that any moiré observed will have a small magnitude or small magnification. We find that a light weight diffuser such as Grafix Matte Acetate 0.005 works well for LCD panels with a pixel pitch in the $\frac{1}{4}mm$ range.

5. Conclusion

In this work, we have described practical methods for the graphics or display researcher to construct ray-based light field displays capable of supporting, and benefiting from, the most recent work in computational and compressive display. It is our hope to inspire future research into new possibilities for glasses-free 3D displays based on simple ray optics, thanks to the increasingly low cost of high performance computing.

References

[1] Lippmann G 1908 *Journal of Physics* **7** 821–825
[2] Ives F E 1903 Parallax stereogram and process of making same U.S. Patent 725,567
[3] Wetzstein G, Lanman D, Hirsch M and Raskar R 2012 *ACM Trans. Graph.* **31** 1–11
[4] Lanman D, Wetzstein G, Hirsch M, Heidrich W and Raskar R 2011 *ACM Trans. Graph.* **3**(6) 1–9
[5] Hutley M C, Hunt R, Stevens R F and Savander P 1994 *Pure and Applied Optics: Journal of the European Optical Society Part A* **3** 133 URL `http://stacks.iop.org/0963-9659/3/i=2/a=006`
[6] Harrold J, Wilkes D and Woodgate G 2004 *Proc. IDW* vol 11 pp 1495–1496
[7] Perlin K, Paxia S and Kollin J S 2000 *ACM SIGGRAPH* pp 319–326
[8] Kim Y, Kim J, Kang J M, Jung J H, Choi H and Lee B 2007 *Optics Express* **15** 18253–18267
[9] Bell G P, Craig R, Paxton R, Wong G and Galbraith D 2008 *SID Digest* **39** 352–355
[10] Lanman D, Hirsch M, Kim Y and Raskar R 2010 *ACM Trans. Graph.* **29**(6) 163:1–163:10
[11] Gotoda H 2010 *SPIE Stereoscopic Displays and Applications XXI* vol 7524 pp 1–8
[12] Gotoda H 2011 *SPIE Stereoscopic Displays and Applications XXII* vol 7863 pp 1–7
[13] Andersen A and Kak A 1984 *Ultrasonic Imaging* **6** 81–94
[14] Wetzstein G, Lanman D, Heidrich W and Raskar R 2011 *ACM Trans. Graph.* **30**(4) 1–11
[15] Davis J A, McNamara D E, Cottrell D M and Sonehara T 2000 *Applied Optics* **39** 1549–1554
[16] Friedlander M P and Hatz K 2008 *Computational Optimization and Applications* **23** 631–647
[17] Oster G, Wasserman M and Zwerling C 1964 *JOSA* **54** 169–175